Self-consistent solution for a collisionless plasma slab in motion across a magnetic field

Marius M. Echim[a)]
Institute of Space Sciences, Atomiştilor 409, P.O. Box MG-23, R-77125 Bucureşti, Romania

Joseph F. Lemaire
Center for Space Radiation, Université Catholique de Louvain Chemin du Cyclotron 2, Louvain-la-Neuve, Belgium

Michel Roth
Institut d'Aéronomie Spatiale de Belgique, Avenue Circulaire 3, Bruxelles, Belgium

(Received 1 February 2005; accepted 10 May 2005; published online 7 July 2005)

The problem of the dynamics of a plasma slab moving across a magnetic field is treated in the framework of the kinetic theory. A velocity distribution function (VDF) is found for each plasma species, electrons and protons, in terms of the constants of motion defined by the geometry of the problem. The zero- and first-order moments of the VDF are introduced into the right-hand side term of Maxwell's equations to compute the electric and magnetic vector potentials and corresponding fields. The solutions are found numerically. We obtain a region of plasma convection—the slab proper—where the plasma moves with a uniform velocity, $V_x = V_0 = (\boldsymbol{E} \times \boldsymbol{B}/B^2)_x$. At the core margins two plasma "wings" are formed, each being the result of a pair of interpenetrated boundary layers with different transition lengths. Inside these wings, the plasma velocity is not uniform, $V_x \neq (\boldsymbol{E} \times \boldsymbol{B}/B^2)_x$. It decreases from the maximum value obtained in the core to a minimum value in the central region of the wings where a flow reversal is found with the plasma convecting in the opposite direction to the core motion. There is also an asymmetry of the velocity gradient at the borders of the core, which results in a corresponding asymmetry in the thickness of the wings. Furthermore, it is found that the reversed plasma flow in the thinner wing is larger than that in the broader wing. For a fixed direction of the magnetic field the two plasma wings interchange position with respect to the center of the slab when the plasma bulk velocity reverses sign. © *2005 American Institute of Physics*.
[DOI: 10.1063/1.1943848]

I. INTRODUCTION

The study of plasma motion across a magnetic field has direct application in many areas of plasma physics, from the study of astrophysical and solar terrestrial plasma flows to laboratory and tokamak experiments. In recent laboratory experiments with plasma guns (see Refs. 1 and 2) or in confining devices such as tokamaks (see Refs. 3 and 4), the propagation of plasma density inhomogeneities (or blobs) turns out to be an important factor for mass and energy transport. On the other side, various models/mechanisms have been proposed to represent the interaction between the solar wind plasma inhomogeneities and the geomagnetic field that takes place at the magnetopause (for a review see Ref. 5). The physical processes that govern this interaction are not yet comprehensively modeled.

Significant advances in this field of investigation are due to the numerical simulations based on the particle-in-cell (PIC) method. They provide solutions for the plasma streaming across the magnetic field in one[6,7] or two dimensions.[8] Neubert *et al.*[9] and Nishikawa[10] developed electrostatic PIC codes that simulate the dynamics of a three-dimensional (3D) plasma cloud across a magnetic field in vacuum as well as in a background plasma. In these simulations the electron to proton mass ratio ($\gamma = m_e/m_p$) is altered by orders of magnitude in order to keep the problem tractable with modern computer resources. The difficulties introduced in PIC simulations by a too small value γ are avoided in the case of an electron-positron plasma[11] where $\gamma = 1$.

Plasma kinetic theory has provided steady-state Vlasov equilibrium solutions for boundary layers forming one-dimensional tangential discontinuities (TDs). Solutions for TDs at the interface between stagnant plasma regions with different temperatures and/or densities were found by Sestero[12] and Lemaire and Burlaga.[13] One-dimensional TD equilibrium solutions at the interface between moving plasma regions were given by Sestero[14] and Roth.[15] Kinetic solutions for one-dimensional TDs with both shears in the magnetic field and plasma bulk velocity are described by Roth,[16] Roth *et al.*,[17] and Lee and Kan.[18]

Echim[19] found that the solutions proposed for steady-state one-dimensional TDs can be used to construct steady-state 2D kinetic solutions describing a nonuniform streaming of a plasma across a magnetic field. In the following we outline an application of this kinetic solution to the motion of a collisionless plasma slab moving in an x direction perpendicularly to background magnetic field lines. The external B field, $\boldsymbol{B}_0 \equiv (0,0,B_0)$, is aligned along the positive z axis, as

[a)]Electronic mail: echim@venus.nipne.ro

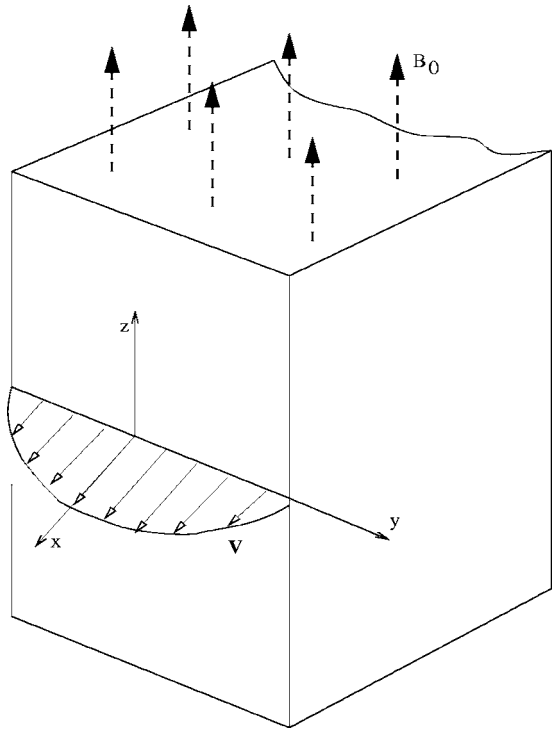

FIG. 1. Schematic 3D plot of an ideal, rectangular, moving plasma slab. Dashed arrows illustrate the distribution of the external magnetic field lines. The 2D plot in front of the slab shows the plasma bulk velocity $V(y)$. The slab is assumed infinite in x and z directions.

illustrated in Fig. 1. We consider 2D spatial variations in the y-z plane (perpendicular to the slab motion) for plasma and field parameters. Echim[19] has shown that in this geometry internal currents are aligned along the x axis, producing therefore magnetic field perturbations only in the y-z plane. These magnetic perturbations add to $\boldsymbol{B}_0$ to produce a total magnetic field $\boldsymbol{B}=[0,B_y(y,z),B_z(y,z)]=[0,b_y(y,z),B_0+b_z(y,z)]$, where $b_y(y,z)$ and $b_z(y,z)$ are the components of the magnetic perturbations produced by the internal plasma currents. The plasma slab considered here is parallel to the external magnetic field and is infinitely long in the x and z directions. It moves in the x direction with a bulk velocity $\boldsymbol{V}=[V_x(y,z),0,0]$ illustrated in Fig. 1.

The paper is organized as follows. Section II describes the velocity distribution function (VDF) of each species (electrons and protons). The zero- and first-order moments are analytically computed in terms of the electric potential $\Phi(y,z)$ and the x component of the magnetic vector potential $A_x(y,z)$. The method to solve the steady-state Maxwell's equations is also discussed. Section III focuses on the numerical results obtained in two cases: (A) a plasma blob moving in the positive direction of Ox across a given external magnetic field $\boldsymbol{B}_0$ and (B) a plasma motion in the negative direction of Ox across the same external magnetic field as in case (A). Section IV summarizes the results and outlines the aspects important for the general problem of plasma motion across B fields.

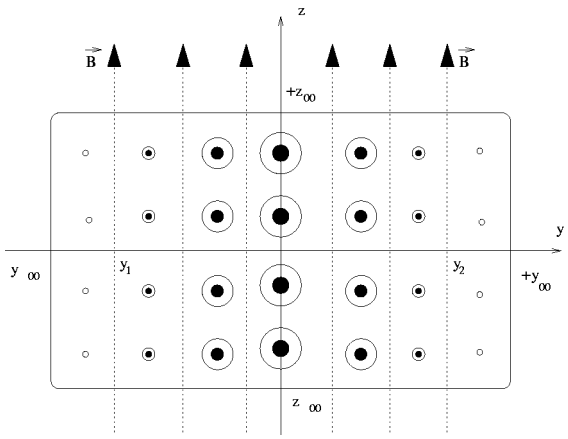

FIG. 2. Cross section normal to the direction of the plasma bulk velocity $\boldsymbol{V}$. The slab is parallel to the plane $y=0$. Plasma bulk velocity is illustrated by circles having the diameter proportional to $V_x(y,z)$ (empty circles correspond to zero velocity). Dotted lines illustrate the distribution of the external magnetic field $\boldsymbol{B}_0$.

II. KINETIC SOLUTION AND SELF-CONSISTENT FIELDS

We assume that the slab motion is not self-sustained, i.e., an external mechanism drives the flow pattern $\boldsymbol{V}=[V_x(y,z),0,0]$ and maintains it in a steady state ($\partial V_x/\partial t=0$). Examples of external drivers sustaining plasma flows of this type are the following: the inertia of excess momentum plasmoids hitting the dayside terrestrial magnetosphere,[20] the initial momentum push imparted by plasma guns used in laboratory experiments (see, for instance, Ref. 1), or the centripetal force in curved geometry of tokamak.[4] The variation of plasma properties and fields with the x coordinate is neglected in this study.

A. Solution of the stationary Vlasov equation

In the absence of collisions and for a time independent problem, the VDF of each plasma component species f_α satisfies the stationary Vlasov equation:

$$\boldsymbol{v}\cdot\frac{\partial f_\alpha}{\partial \boldsymbol{r}}+\frac{q_\alpha}{m_\alpha}(\boldsymbol{E}+\boldsymbol{v}\times\boldsymbol{B})\cdot\frac{\partial f_\alpha}{\partial \boldsymbol{v}}=0. \tag{1}$$

In Eq. (1) the electromagnetic field on the left-hand side (lhs) includes the internal plasma contribution determined by the electric charge density ($q_\alpha n_\alpha$) and the current density ($\boldsymbol{J}_\alpha=q_\alpha n_\alpha \boldsymbol{u}_\alpha$) of each plasma species ($\boldsymbol{u}_\alpha$ is the average velocity of species α); they are derived from the moments of f_α.

The characteristic curves of Eq. (1) correspond to the trajectories of the particle with charge q_α and mass m_α that moves into the electromagnetic field given by the distributions $\boldsymbol{E}(\boldsymbol{r})$ and $\boldsymbol{B}(\boldsymbol{r})$.[21] Thus the solution of Eq. (1) can be any positive, real function of the constants of motion. The solution of Eq. (1) has also to satisfy asymptotic boundary conditions imposed at infinity or at large distances along the parallelepipedal surface illustrated in Figs. 1 and 2.

The symmetry of the problem does not eliminate the dependence of f_α on any of the three components of the velocity, v_x, v_y, v_z. Therefore the solution must be given in terms of the three constants of motion. Since the electromag-

netic field does not depend on time, the electric field can be derived from a scalar potential $\Phi(y,z)$, and the total energy of the particle α is a constant of motion: $H=(1/2)m_\alpha(v_x^2+v_y^2+v_z^2)+q_\alpha\Phi$.

Since the x coordinate is ignorable, the corresponding component of the canonical momentum, $p_x=m_\alpha v_x+q_\alpha A_x(y,z)$, is a constant of motion. In the special case when the component of the magnetic vector potential, A_x, does not depend on z (as in one-dimensional models of TDs), the third constant of motion is equal to p_z.[12–17]

Since the assumption that the z coordinate is ignorable is not *a priori* justified, we will assume that the spatial variation of the electromagnetic field is smooth enough such that the Alfven conditions[22] are satisfied and $r_{L\alpha}|\nabla B|\ll B$, where $r_{L\alpha}$ is the radius of gyration of the particle α. Thus the magnetic moment of the particle, $\mu_\alpha=m_\alpha w_\perp^2/2B$, is an adiabatic invariant; $w_\perp$ is the perpendicular component of the particle velocity in the reference frame moving with the zero-order drift velocity, $\boldsymbol{U}_E=(\boldsymbol{E}\times\boldsymbol{B})/B^2$. Instead of p_z we use, in the more general 2D case, the magnetic moment μ_α as a third (approximate) constant of motion. The magnetic moment has been successfully used in previous kinetic models such as, for instance, in the study of the radiation belt particles and in the exospheric models of the solar and polar winds (see Ref. 23).

To summarize, we consider two exact constants of motion: (**i**) the total energy H and (**ii**) the p_x component of the canonical momentum. The third constant of motion is approximated by an adiabatic invariant: (**iii**) the magnetic moment. Any positive real function $f_\alpha(H,p_x,\mu)$ is a solution of the Vlasov equation (1). This solution has to satisfy the boundary conditions described below.

The solution is searched inside the parallelepiped shown in Fig. 1 whose cross section is the rectangle $\Gamma=[-y_\infty,+y_\infty]\times[-z_\infty,+z_\infty]$ illustrated in Fig. 2; y_∞ and z_∞ are finite distances that are still large compared to the proton Larmor radius. The plasma bulk velocity has nonzero values inside a finite domain $y\in[y_1,y_2]$, with $[y_1,y_2]\subset[-y_\infty,+y_\infty]$; $V_x(y,z)$ decreases to zero for $y\to\pm y_\infty$ (see Fig. 2). Note that, in this paper, we do not impose any variation of V_x with the z coordinate at the edges of the plasma slab.

The VDF satisfies the following boundary conditions:

$$\lim_{y\to+y_\infty} f_\alpha=f_{\alpha1},\qquad \lim_{y\to-y_\infty} f_\alpha=f_{\alpha1}, \tag{2}$$

where $f_{\alpha1}$ is an isotropic Maxwellian that corresponds to an equilibrium stagnant plasma with density $N_{\alpha1}$ and temperature $T_{\alpha1}$:

$$f_{\alpha1}(p_x,\mu,H)=N_{\alpha1}\left(\frac{m_\alpha}{2\pi KT_{\alpha1}}\right)^{3/2}e^{-H/KT_{\alpha1}}. \tag{3}$$

An admissible solution satisfying condition (2) is given below:

$$f_\alpha(p_x,\mu,H)=g_\alpha(p_x)f_{\alpha1}(p_x,\mu,H)+h_\alpha(p_x)f_{\alpha2}(p_x,\mu,H), \tag{4}$$

where the following functions were defined at $y=0$:

$$f_{\alpha2}(p_x,\mu,H)=N_{\alpha2}\left(\frac{m_\alpha}{2\pi KT_{\alpha2}}\right)^{3/2}e^{-\left(H-p_xV_0+\frac{1}{2}m_\alpha V_0^2\right)/KT_{\alpha2}}, \tag{5}$$

$$g_\alpha(p_x)=\eta[\mathrm{sgn}(q_\alpha)(p_x-q_\alpha A_{x1})]+\eta[-\mathrm{sgn}(q_\alpha)(p_x-q_\alpha A_{x2})], \tag{6}$$

$$h_\alpha(p_x)=\eta[\mathrm{sgn}(q_\alpha)(p_x-q_\alpha A_{x2})]-\eta[\mathrm{sgn}(q_\alpha)(p_x-q_\alpha A_{x1})], \tag{7}$$

with η being the Heaviside step function and sgn the signum function.

The function $f_{\alpha2}$ corresponds to a displaced Maxwellian that describes a plasma whose average velocity in the Ox direction is equal to V_0. The truncation functions $g_\alpha(p_x)$ and $h_\alpha(p_x)$ are defined such that in the (H,p_x) space the contribution of $f_{\alpha2}$ to the VDF is limited to the region where $p_x\in[q_\alpha A_{x2},q_\alpha A_{x1}]$ with $A_{x1}=-B_0y_1$, $A_{x2}=-B_0y_2$ for $\forall\ z\in[-z_\infty,+z_\infty]$. The two free input parameters y_1 and y_2 satisfy the inequality $y_1<0<y_2$ and specify the y coordinate where the transition from moving to stagnant regime takes place at the two sides of the slab. Since the reference system is chosen such that the external magnetic field $\boldsymbol{B}_0$ is parallel to z axis and positive $A_{x2}<A_{x1}$.

Thus these boundary conditions correspond to uniform magnetic field at the left and right edges of the plasma slab: $\boldsymbol{B}(y\to-y_\infty)=\boldsymbol{B}(y\to+y_\infty)=\boldsymbol{B}_0$, equal to the external magnetic field. The imposed boundary conditions for the plasma flow and magnetic field at the left and right edges of the plasma slab do not require any variation with the spatial z coordinate. This will result in very slight variations of the different plasma and field parameters in the z direction, as shown in the forthcoming numerical results. Note also that the expression (4) for $f_\alpha(H,p_x)$ does not depend on μ. Only the domains of integration of f_α in (H,p_x,μ) space depend on the third constant of motion μ.

B. Moments of the VDF

The moments of the VDF determine the electric charge and current densities for each plasma component.[24] The general expression for the rst moment of the VDF is given by

$$Q_\alpha^{rst}(\boldsymbol{r},t)=\int\int\int v_x^r v_y^s v_z^t f_\alpha d^3\boldsymbol{v}. \tag{8}$$

The moments will be computed by an integration in the space of the constants of motion (H,p_x,μ). The charge density of each plasma component is equal to

$$\rho_\alpha=q_\alpha Q_\alpha^{000}=\int_{-\infty}^{+\infty}\int_{H_{c\alpha}}^{+\infty}\int_{\mu_{c\alpha}}^{+\infty} f_\alpha(H,p_x,\mu)\times\left|\frac{D(v_x,v_y,v_z)}{D(H,p_x,\mu)}\right|d\mu\,dp_x dH. \tag{9}$$

The integration is carried out in the (H,p_x,μ) space. The Jacobian of the transformation from the (v_x,v_y,v_z) variables to (H,p_x,μ) given by

$$\mathcal{J}=\left|\frac{D(v_x,v_y,v_z)}{D(H,p_x,\mu)}\right|=\frac{\sqrt{B_0}}{2m_\alpha^2\sqrt{\mu-\mu_{c\alpha}}\sqrt{H-H_{c\alpha}}}$$

has been introduced in Eq. (9). The lower limits of integration, $H_{c\alpha}$ and $\mu_{c\alpha}$, are determined by the condition of accessibility of particles coming from $\pm y_\infty$. The accessibility conditions for various profiles of the electric potential have been discussed in Refs. 23, 25, and 26. These conditions coincide with the conditions for the Jacobian to have real values. They were derived by Echim:[19]

$$H_{c\alpha}(p_x,\mu)=\mu B+(p_x-q_\alpha A_x)U_E+q_\alpha\Phi-\frac{m_\alpha U_E^2}{2}, \quad (10)$$

$$\mu_{c\alpha}(p_x)=\frac{m_\alpha}{2B}\left(\frac{p_x-q_\alpha A_x}{m_\alpha}-U_E\right)^2, \quad (11)$$

where $\boldsymbol{U}_E=(\boldsymbol{E}\times\boldsymbol{B})/B^2$. The analytical integration gives the following expression for the charge densities of electrons ($\alpha=e$) and protons ($\alpha=p$):

$$\rho_\alpha(\Phi,A_x)=\rho_{\alpha1}(\Phi,A_x)+\rho_{\alpha2}(\Phi,A_x), \quad (12)$$

where the two functions $\rho_{\alpha1}(\Phi,A_x)$ and $\rho_{\alpha2}(\Phi,A_x)$ are specified in Appendix A.

The current density for each species is determined by the first-order moment of the VDF. For a plasma flow parallel to the Ox axis, $Q^{010}=Q^{001}=0$. Thus the only nonvanishing component of the current is equal to

$$j_{x\alpha}=q_\alpha Q_\alpha^{100}=\int_{-\infty}^{+\infty}\int_{H_{c\alpha}}^{+\infty}\int_{\mu_{c\alpha}}^{+\infty}\left(\frac{p_x-q_\alpha A_x}{m_\alpha}\right)f_\alpha(H,p_x)\times\left|\frac{D(v_x,v_y,v_z)}{D(\mu,H,p_x)}\right|d\mu\,dH\,dp_x. \quad (13)$$

After analytical integration of (13) over the accessible domains in the (H,p_x,μ) space, the current density can be written as

$$j_{x\alpha}(\Phi,A_x)=j_{x\alpha1}(\Phi,A_x)+j_{x\alpha2}(\Phi,A_x), \quad (14)$$

where the functions $j_{x\alpha1}(\Phi,A_x)$ and $j_{x\alpha2}(\Phi,A_x)$ are specified in Appendix A.

C. Self-consistent electromagnetic potentials and fields

The electromagnetic potentials satisfy the Maxwell's equations

$$\nabla^2\Phi=-\frac{1}{\epsilon_0}\sum_\alpha\rho_\alpha, \quad (15)$$

$$\nabla^2\boldsymbol{A}=-\mu_0\sum_\alpha\boldsymbol{j}_\alpha. \quad (16)$$

The assumptions made on the symmetry of the sheared flow ($\partial/\partial t=0$, $\partial/\partial x=0$) specify that the electromagnetic field distribution has to satisfy the following constraints:

TABLE I. Boundary conditions for the plasma bulk velocity and the magnetic vector potential imposed on the borders of the rectangular domain Γ shown in Fig. 2. Note that B_0, the magnitude of the external magnetic field, is an input parameter while $V_B(y)$ is self-consistently determined.

Boundary	$y=-y_\infty$	$y=+y_\infty$	$z=-z_\infty$	$z=+z_\infty$
V_x	0	0	$V_B(y)$	$V_B(y)$
A_x	B_0y_∞	$-B_0y_\infty$	$-B_0y$	$-B_0y$

$$\boldsymbol{E}\equiv[0,E_y(y,z),E_z(y,z)],\quad \boldsymbol{B}\equiv[0,B_y(y,z),B_z(y,z)]. \quad (17)$$

Without loss of generality the magnetic field distribution (17) can be obtained from a magnetic vector potential whose only nonvanishing component is $A_x(y,z)$. The Dirichlet boundary conditions for A_x are specified in Table I giving a boundary magnetic field equal to the external field, $\boldsymbol{B}_0$.

It is known that the plasma always tends to a state of electric quasineutrality. A net electric charge is effectively screened by collective effects at distances larger than the Debye length $\lambda_D=\sqrt{\epsilon_0KT/2ne^2}$. Since in this study we consider flows whose characteristic scale length for spatial variation is much larger than λ_D, one can assume that the quasineutrality condition is satisfied. The electric potential is then computed from the condition that the total number of electrons is everywhere equal to the total number of positive charges:

$$\sum_\alpha\rho_\alpha[\Phi(y,z),A_x(y,z)]=0, \quad (18)$$

with the charge density of species α given by Eq. (12). Equations (16) and (18) together with the analytical expressions of the moments (12)–(14) and the Vlasov solution (4) fully determine the self-consistent solution of the electromagnetic field.

The two equations (16) and (18) are discretized on the uniform mesh defined for the domain Γ. The numerical solution is computed by an iterative method: an initial guess for $A_x(y,z)$ is introduced into the nonlinear algebraic equation (18) whose solution $\Phi(y,z)$ is found by a bisection numerical method at each point of the grid. This electric potential is then introduced into the discrete partial derivatives equation (16) whose solution gives the magnetic vector potential at all grid points. The latter equation is solved with a finite difference preconditioned Gauss-Seidel method. Its solution $A_x(y,z)$ is introduced in the quasineutrality equation (18) and an updated electric potential $\Phi(y,z)$ is found. The procedure is repeated over and over until this iterative process converges to the solution, i.e., when differences between two consecutive steps become smaller and smaller at all grid points. In the following section we show a numerical example with plasma parameters typical for the region of interaction between the solar wind and the terrestrial magnetosphere. The convergence is reached after 15 iterations in both the cases discussed below.

TABLE II. Boundary values, scaling factors, and their physical units, used as input parameters in the numerical solutions considered in the two cases discussed in Sec. III. $N_{1e}=N_{2e}$ and $N_{1p}=N_{2p}$.

	B_0 (nT)	λ_B (nT)	N_0 (cm^{-3})	N_{1e} (cm^{-3})	N_{1p} (cm^{-3})	$T_{\rm ref}$ (eV)	T_{e1} (eV)	T_{p1} (eV)	T_{e2} (eV)	T_{p2} (eV)	β	V_0 (km/s)	λ_D (m)	$r_{\rm Lp}$ (km)	λ_Φ (V)	λ_V (km/s)	y_∞ (km)	z_∞ (km)	y_1 (km)	y_2 (km)
(A)	10^2	10^3	1	3	3	1.5	150	5	150	15	0.018	55	3.71	1.77	1	13.3	354	70	−177	+177
(B)	10^2	10^3	1	3	3	1.5	150	5	150	15	0.018	−55	3.71	1.77	1	13.3	354	70	−177	+177

III. NUMERICAL SOLUTION: AN EXAMPLE

The numerical method described above has been applied to a dimensionless form of Eqs. (12), (14), (16), and (18). The scaling factors for lengths, densities, fluxes, bulk velocities, magnetic and electric fields, and potentials that are used to normalize the equations are specified in Appendix B. The lengths and the velocities are scaled, respectively, with $r_{\rm Lp}$ the proton Larmor radius and $V_{\rm Tp}$ the proton thermal velocity corresponding to the reference energy ($KT_{\rm ref}$) of 1.5 eV. The rationale of this scaling is that we are interested in solutions for a plasma slab whose scale length is larger than $r_{\rm Lp}$ (i.e., we work in the so-called small Larmor radius beam approximation, see Ref. 27).

The results shown in this section were obtained under the cold plasma approximation, i.e., the asymptotic temperature of proton population is smaller than the asymptotic temperature of the electron population within the plasma slab as well as at large distances from it:

$$T_{p1} < T_{e1}, \quad T_{p2} < T_{e2}.$$

Furthermore, in this first application we consider the case when the slab plasma is warmer than the background plasma ($T_{p1} < T_{p2}$). The slab moves with a sheared convection velocity $V_x(y,z)$ parallel to the Ox axis and perpendicular to the external magnetic field $\boldsymbol{B}_0$, which is parallel to the Oz axis at a large distance from the plasma slab. Furthermore, we restrict this numerical application to the case of a low-β plasma.

A. Plasma slab moving with positive velocity: $V_0>0$

In order to point out the effects due to the relative motion between the plasma slab and the background plasma, the density (of electrons and protons) in the middle plasma slab ($N_{i2}=N_{e2}$) is equal to that of the stagnant background plasma ($N_{i1}=N_{e1}$) and take values generally encountered in the outer layers of the terrestrial magnetosphere. We consider a moving plasma slab ($V_0=+55$ km/s) with slightly greater temperatures than the background plasma. The position of the region of transition from moving to stagnant regime is determined by $y_2=-y_1=100r_{\rm Lp}$. The magnitude of the external magnetic field is equal to $B_0=100$ nT. A summary of the input parameters is given in Table II.

The plasma moves in the x direction and its bulk velocity is given by the center-of-mass speed:

$$V_x(y,z)=\frac{m_p Q_p^{100}(\Phi,A_x)+m_e Q_e^{100}(\Phi,A_x)}{m_p Q_p^{000}(\Phi,A_x)+m_e Q_e^{000}(\Phi,A_x)}, \tag{19}$$

where m_p and m_e are the proton and electron masses. Figure 3 shows the asymmetric distribution of V_x obtained inside the rectangle Γ. The plasma has a roughly uniform bulk velocity in the positive direction of the x axis within a core region bounded by $y_{\rm LA}\approx -20r_{\rm Lp}$ and $y_{\rm RA}\approx +40r_{\rm Lp}$ and extending all along z. The core's width is approximately equal to 100 km. This sheared profile of the convection velocity corresponds fairly well to the slab geometry described in the Introduction.

One notable feature of the self-consistent profile is the formation of two wings or boundary layers at the edges of the moving slab. The bulk motion of the plasma slab in the positive direction of the x axis drives the background plasma to move in the opposite direction, like a piston or a bar impinging into a stagnant fluid. The profile of the plasma bulk velocity is asymmetric with respect to the center of the slab ($y=0$). The boundary layer formed at the right-hand side (rhs) of the slab ($y>y_{\rm RA}$) is much thinner than the layer at the left ($y<y_{\rm LA}$). The gradient of the plasma velocity is also

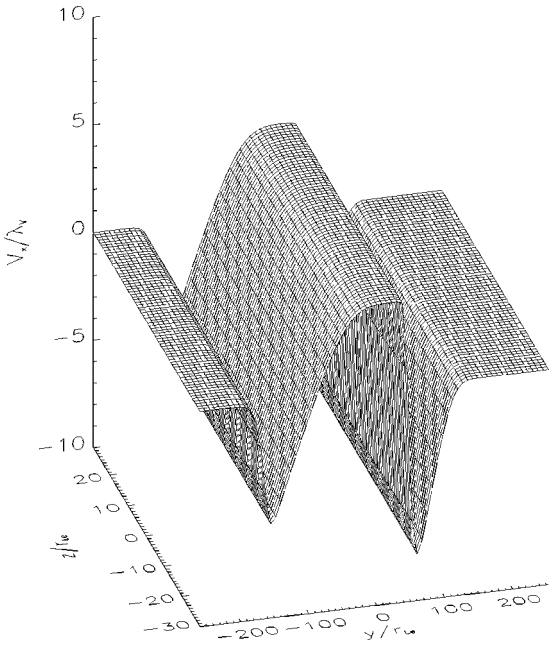

FIG. 3. Case (A)—Distribution of the V_x/V_0 plasma bulk velocity vs $y/r_{\rm Lp}$ and $z/r_{\rm Lp}$. Two "wings" are formed on both sides of the moving slab; the thinner is localized on the rhs of the slab.

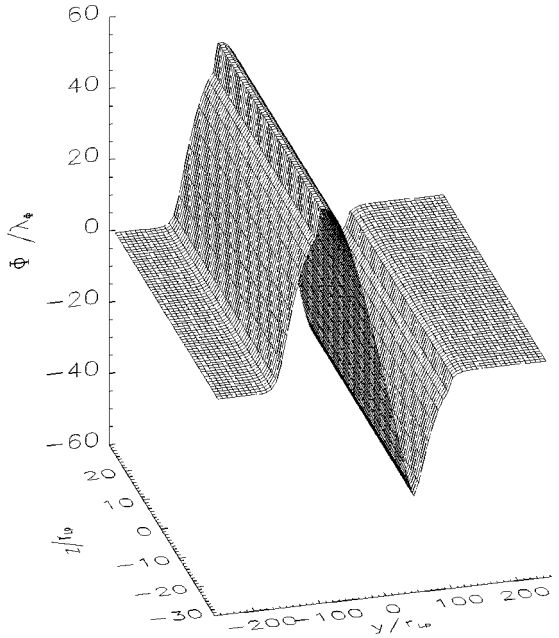

FIG. 4. Case (A)—Distribution of $\Phi(y,z)$, the electric potential, solution of Eq. (18).

stronger on the rhs of the slab. In the remainder these two large-scale boundary structures will be called "plasma sheaths" (PSs).

Figure 4 shows the distribution of the electrostatic potential given by the solution of the quasineutrality equation (18). In addition to the two PSs obtained for the distribution of $V_x(y,z)$, the distribution of $\Phi(y,z)$ reveals smaller scale structures. Indeed, the electric potential has two sharp jumps at $y=y_1$ and $y=y_2$ within two microscale sheets embedded into the two large-scale PSs. Note that y_1 and y_2 are different

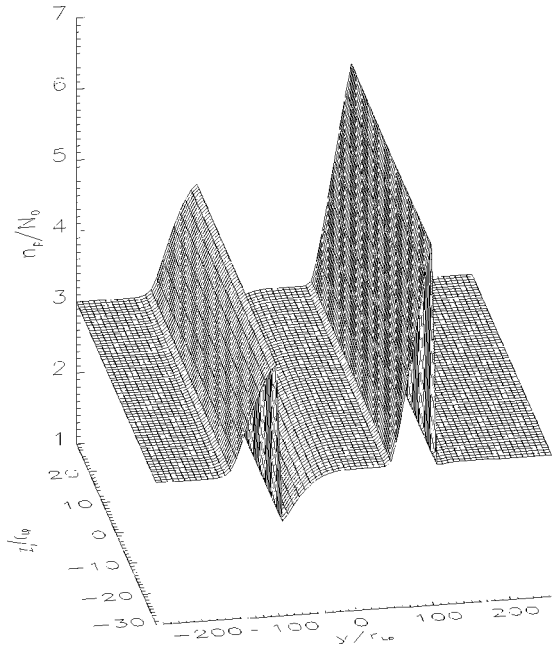

FIG. 5. Case (A)—Normalized number density of the protons. Since the quasineutrality condition is satisfied, the same profile is obtained for the electrons ($n_i=n_e$).

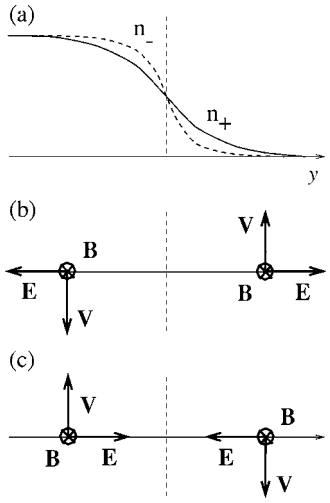

FIG. 6. The response of ions and electrons in a TD depends on the sense of the flow shear on either side of the layer [from the work of De Keyser and Roth (Ref. 31)]. In a unidirectional magnetic field $\boldsymbol{B}$ (pointing inside the paper), one sense of the shear flow $\boldsymbol{V}$ gives rise to an electric field $\boldsymbol{E}$ directed away from the center of the layer (b). $\boldsymbol{E}$ tends to pull the protons in the outer fringes of the TD out of the layer (a) while the number densities of protons (solid line) and electrons (dashed line) to the left of the TD gradually vanish across the layer. The protons are indeed expected to penetrate furthest onto the other side of the transition because of their larger gyroradius. Note that in (a) the protons and electrons originating from the right side are not shown [in the work of De Keyser and Roth (Ref. 31), they are symmetric with respect to the center of the layer]. (c) For the opposite flow sense, electrons are pulled out of the layer.

from y_{RA}, y_{LA}. The former are input parameters of the Vlasov solution (4) and correspond to the centers of the two regions of transition from moving plasma (described by $f_{\alpha 2}$) to stagnant plasma (described by $f_{\alpha 1}$); y_{RA}, y_{LA} are output values obtained in the numerical solution of case (A), delimiting the core region where the plasma bulk velocity is uniform.

The four different transition lengths discussed above are also illustrated in Fig. 5 showing the ion density structure. They can be divided into external pairs of embedded transition layers resulting from the interpenetration of the moving plasma slab and the stagnant plasma. The first external pair of transition layers occurs at the lhs of the moving plasma slab. It is characterized by a smooth increase of the density with a transition length on the order of the cold background proton gyroradius—the PSs. It extends from $y\approx -190r_{Lp}$ to $y=y_{LA}$. This PS is interpenetrated by a thin current sheet (CS) centered on $y=y_1$ where the density decreases sharply within a layer whose transition length is of the order of the hot plasma slab electron gyroradius. The second external plasma sheath/current sheet (PS/CS) pair occurs at the rhs of the moving plasma slab. It is characterized by a smooth increase of the density with a transition length on the order of the hot plasma slab gyroradius—the right-hand side PS. It extends from $y=y_{RA}$ to $y=y_2$. It is followed by a sharp decrease of the density with a transition length on the order of the cold background electron gyroradius (the right-hand side CS).

The different scale lengths obtained on both sides of the moving plasma slab confirm the profiles of the classical so-

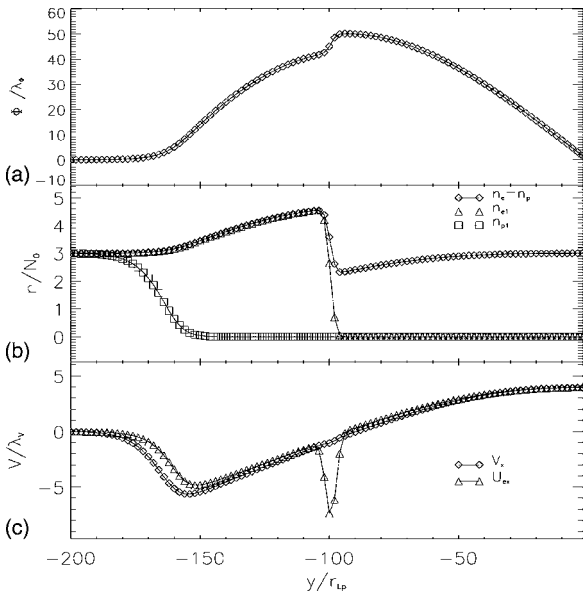

FIG. 7. Case (A)—Detail distributions of several plasma parameters inside the plasma sheath on the left-hand side for $z=0$: (a) upper panel—normalized electric potential; (b) middle panel—normalized density (n_i and n_e are the total number densities of the ions and electrons; n_{i1} and n_{e1} are the partial ion and electron densities of the lhs stagnant population); (c) lower panel—normalized plasma bulk velocity.

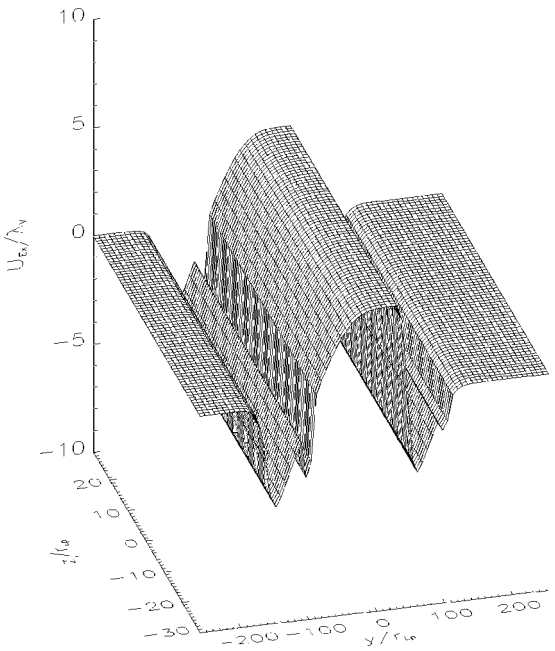

FIG. 8. Case (A)—Distribution of U_E the electric drift velocity, computed from the solutions of Eqs. (16) and (18). Note that V_x the plasma bulk velocity is approximately equal to U_E only in the center core of the slab.

lutions for 1D tangential discontinuities computed by Sestero,[14] Roth,[15,16] Kuznetsova *et al.*,[28] and De Keyser and Roth.[29–32] The variable scaling at the two sides is due to the electric field inside the layer as illustrated by Fig. 6 (from the work of De Keyser and Roth[31]) showing a schematic representation of a TD layer formed by the interpenetration of two identical plasma regions in relative motion across a unidirectional magnetic field.

Between $y=y_1$ and $y=y_2$ the electric potential is decreasing, which indicates an electric field in the direction of the positive y axis (the same orientation as the convection electric field resulting from the geometry of Fig. 2). The electric field inside the plasma slab acts on the hot electrons of its left boundary like the electric field acts on the electrons of the boundary having the shear flow orientation illustrated in part (c) of Fig. 6. Similarly, the electric field inside the plasma slab acts on the hot protons of its right boundary like the electric field acts on the protons of the boundary having the shear flow orientation illustrated in part (b) of Fig. 6. For $y>y_2$, there is a reversal of the electric field in the background plasma left backwards in the negative x direction. For $y>y_2$ the electric field is directed toward the inside of the plasma slab (in the negative y direction) as in case (c) of Fig. 6.

The cold electrons of the right background plasma (moving backwards) are pulled toward the outside of the moving plasma slab. Note that De Keyser and Roth[29] predicts that if the shear flow is too strong, the kinetic energy of the particles (protons for one sense of the shear flow, electrons for the other sense) is not sufficient to overcome the electrostatic energy barrier and no equilibrium is possible. Because of the smaller electron gyroradius, a larger shear flow is needed to set up an energy barrier for the electrons that prohibits equilibrium. This explains why the backward motion of the background plasma is larger at the right edge of the plasma slab than at the left edge.

In Fig. 7 are shown the results from computations performed for a finer grid, limited to the left boundary layer: $y\in[-y_\infty,0]$. The "jump" of the potential noticed at $y=y_1$ is resolved and shown in the upper panel. The upper curve (symbol "◇") of the middle panel of Fig. 7 illustrates the profile of $n_e(y)$ and $n_p(y)$ inside the lhs wing. Note that the curves formed by the symbols "△" and "□" correspond, respectively, to the distributions of electrons (n_{e1}) and protons (n_{p1}) originating from outside the slab, on the lhs at $y=-y_\infty$. The densities of the electrons and protons inside the slab are not shown but are equal to n_e-n_{e1} and n_p-n_{p1}. The sharp variation in the electrostatic potential occurs at the right edge of the first transition layer, which scales with the cold background proton gyroradius. The width of the thin sheet is proportional to the cold electron Larmor radius from the stagnant regime (characterized by n_{e1}). A similar electronic structure is found at $y=y_2$ (not shown).

Both microscale layers coincide with the region of transition of the electron population from the stagnant regime (characterized by the electron density n_{e1}) to the moving regime (characterized by the electron density n_{e2}). A thermal proton incident from the left stagnant plasma that attempts to penetrate into the moving plasma slab has to traverse a region where the electric field repels it: this region constitutes an energy barrier. The height of the energy barrier is proportional to (i) the distance over which the background proton (n_{p1}) density vanishes (with the cold proton Larmor gyroradius as the transition length) and (ii) the electric field (which in turn depends on the shear flow).

In the presence of the magnetic field $\boldsymbol{B}$, the electric field, $\boldsymbol{E}=-\boldsymbol{\nabla}\Phi$, sustains an electric drift (or *convection* velocity)

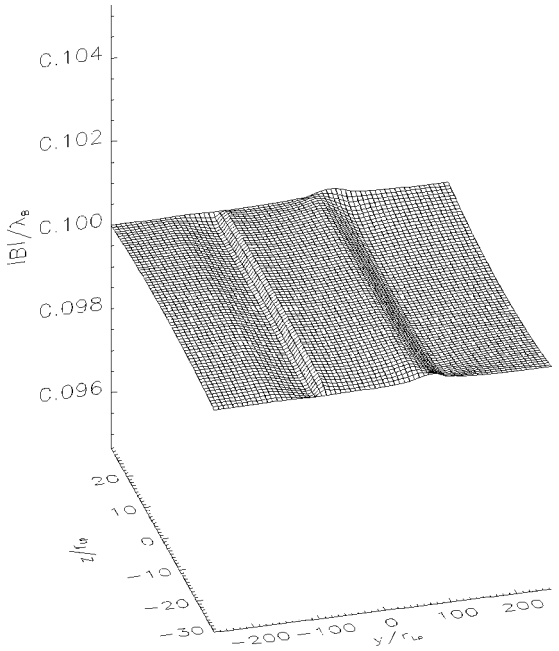

FIG. 9. Case (A)—Total magnetic field B; the external field is slightly altered by the diamagnetic currents carried by the electrons and protons in the ion sheaths and electron sheets.

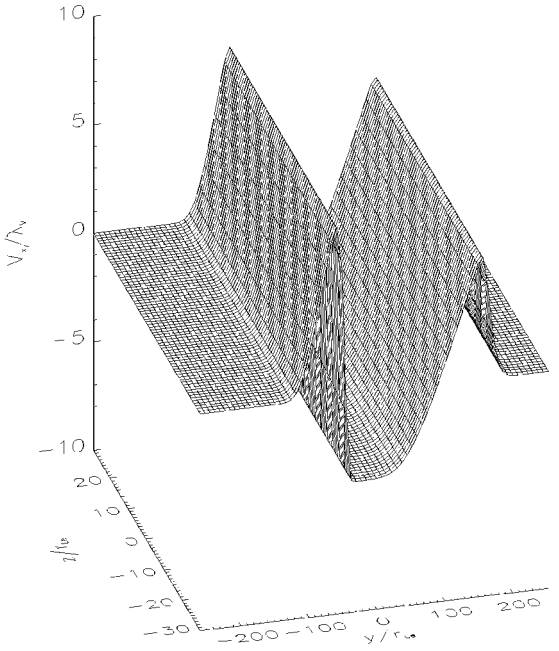

FIG. 10. Case (B)—Distribution of V_x/V_0, the plasma bulk velocity. The core of the slab moves with uniform, negative velocity. Two wings form at the edges of the moving slab where the plasma moves in the direction opposite to the core.

which is equal for the electrons and ions, $\mathbf{U}_E=(\boldsymbol{E}\times\boldsymbol{B})/B^2$. The drift velocity is precisely the ideal magnetohydro dynamics (MHD) convection velocity. For case (A) the nonvanishing component of the drift velocity, U_{Ex}, is shown in Fig. 8. Note that V_x, the bulk velocity of the core of the plasma slab, is almost equal to the convection velocity U_E. This is not true inside the small-scale current sheet at $y=y_1$. Indeed the lower panel of Fig. 7 indicates that the magnitude of the convection velocity U_{Ex} is drastically larger than the magnitude of the plasma bulk velocity inside the microscale CS. It is clear that inside this layer the MHD is badly violated. The increase of the electron pressure inside this microscale sheet produces a sharp gradient of the electric potential. This enhancement of $\boldsymbol{E}$ is associated with a strong electron current intensity and bulk speed of electrons. However, the bulk velocity of the more massive protons is only slightly changed by this rather localized electric field enhancement.

The total current density j_x (not shown) also peaks sharply inside the thin sheet of the external pairs of interpenetrated boundary layers. This diamagnetic current layer produces a slight perturbation of the external magnetic field (less than 10%, see Fig. 9), since the value of β is very small, $\beta=1.81\times10^{-2}$. Also note the slight variation of the magnetic field with z close to the lower and upper borders.

B. Plasma slab moving with negative velocity: $V_0<0$

A second set of numerical results [case (B)] is obtained by changing the sign of the parameter V_0 in Eq. (5) as well as in the expressions (A1), (A2), and (A5), (A6) of the zero- and first-order moments. All the other parameters keep the values used in case (A) (see Table II).

The distribution of the plasma bulk velocity, obtained by the iterative process described above, is shown in Fig. 10; it takes a uniform but negative value, equal to $V_0=-55$ km/s, inside of a core confined in the region limited by $y_{\mathrm{LB}}=-40\ r_{\mathrm{Lp}}$ and $y_{\mathrm{RB}}=20r_{\mathrm{Lp}}$ and extending all along the z direction. As in case (A), the slab proper has two lateral wings within which the plasma bulk velocity changes sign. Note also that the width of the core, $\Delta=y_{\mathrm{RB}}-y_{\mathrm{LB}}$, has the same value ($\approx60r_{\mathrm{Lp}}$) as in case (A).

The PS with a sharper variation of V_x now forms at the lhs of the slab, while on the right-hand side a thicker bound-

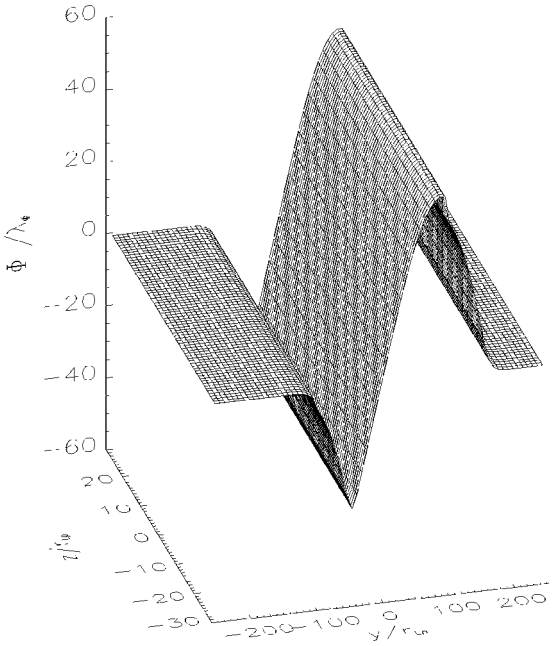

FIG. 11. Case (B)—Distribution of $\Phi(y,z)$ the electric potential obtained from Eq. (18).

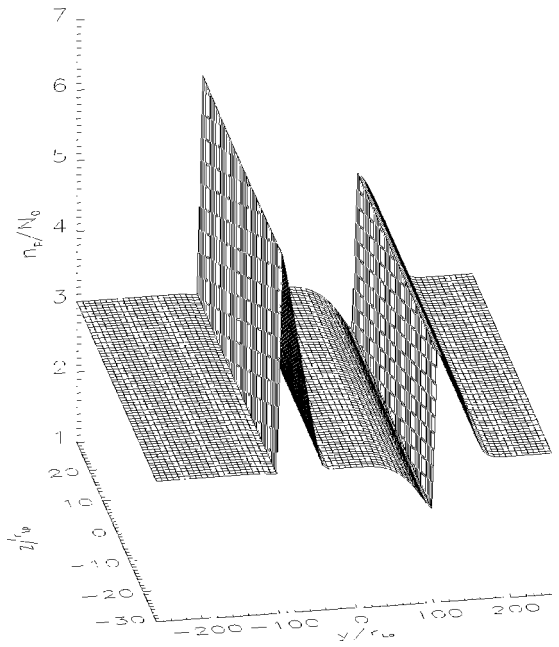

FIG. 12. Case (B)—Normalized number density of the protons. Since the quasineutrality is satisfied, the same density is obtained for the electrons.

ary layer develops with a much smoother gradient for the bulk velocity V_x. This is a direct consequence of the reversal of the sense of the flow which fixes the sign of the electric field as illustrated schematically in Fig. 6.

In case (B) the electrostatic potential first decreases to a minimum value and then has a positive maximum, as shown in Fig. 11. Its values on the two sides of the rectangle are $\Phi(\pm y_\infty)=0$, as expected. The electric field determines an electric drift velocity U_E (not shown) whose value is almost equal to V_x, inside the core. As in case (A), the potential has a sharp gradient within two thin sheets in $y=y_1$ and $y=y_2$.

The total number density of both electrons and protons has again two peaks shown by Fig. 12. The density peak now occurs close to $y_1=-100r_{\mathrm{Lp}}$ while in case (A) the maximum was obtained close to $y_2=+100r_{\mathrm{Lp}}$. By comparison with case (A) one can note the reversal in the positions of these two external boundary layers. The sharpest slope of the plasma density now takes place on the lhs of the moving slab, while in case (A), when the plasma moved in the positive direction, it is found on the right-hand side. As expected, Fig. 12 is the image with respect to the center of the plasma slab of the density structure obtained for $V_0>0$ and illustrated in Fig. 5.

A more closer look of the thin PS formed on the left-hand side is displayed in Fig. 13. The upper panel illustrates the variation of the electric potential with y at $z=0$ (the profile is virtually the same at all z). The density of cold electrons and protons (n_{e1} and n_{p1}) from the left region of the background plasma as well as the total charge density ($n_e=n_p$) are illustrated in the middle panel of Fig. 13. The sharp gradient of the density in $y=y_1$ corresponds to a localized gradient of the electric potential, as in case (A). Note however that the scale length of the left-hand side PS of case (B) is smaller than that of case (A).

For $-105\leqslant y/r_{\mathrm{Lp}}\leqslant -95$ the electric field in the transition layer of the background plasma, moving backwards in the positive direction of the x axis, is directed toward the inside of the moving plasma slab as in case (c) of Fig. 6. The electrons are pulled out of the left transition layer by the inward directed electric field. A cold electron incident from the left stagnant plasma has to overcome a strong electrostatic energy barrier. This produces the sharp increase of the total density between $y/r_{\mathrm{Lp}}\approx -105$ and $y/r_{\mathrm{Lp}}\approx -95$ illustrated in the middle panel of Fig. 13. To maintain charge neutrality hot electrons from the moving plasma slab (not shown) are also pulled toward the outside of the slab to neutralize the cold protons (n_{i1}) pulled toward the inside of the slab between $y/r_{\mathrm{Lp}}\approx -95$ and $y/r_{\mathrm{Lp}}\approx -40$. The lower panel of Fig. 13 shows that inside the microscale sheet, the drift velocity U_E peaks to higher values than the bulk velocity V_x as in case (A).

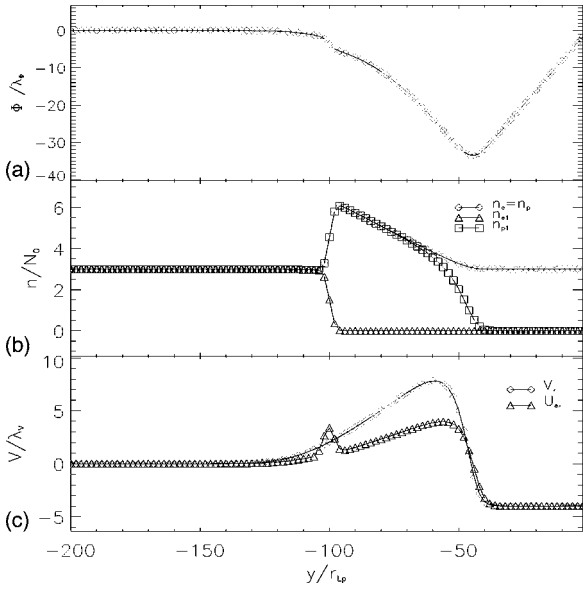

FIG. 13. Case (B)—Detail distribution of several plasma parameters inside the plasma sheath on the lhs for $z=0$: (a) upper panel—normalized electric potential; (b) middle panel—normalized density (n_i and n_e are the total proton and electron densities; n_{i1} and n_{e1} are the proton and electron densities of the stagnant population on the lhs); (c) lower panel—normalized plasma bulk velocity.

IV. DISCUSSION AND CONCLUSIONS

One-dimensional kinetic TD models predict the response of ions and electrons in a tangential discontinuity to depend on the sense of the shear flow on either side of the layer that leads to a variation of the layer's width with the sense of the shear. For similar configurations, hybrid particle simulations by Cargill and Eastman[33] showed that the length scale of the transition in the bulk velocity profile, and, correspondingly, in the density profile, changes with the direction of the flow.

In this paper we have derived a kinetic model for the dynamics of a plasma slab moving across the magnetic field into a colder stagnant plasma. We obtain a region of plasma convection—the slab proper—surrounded by a stagnant plasma. Inside the slab we identify a core where the plasma moves with almost a uniform velocity, $V_x=V_0=(\boldsymbol{E}\times\boldsymbol{B}/B^2)_x$. On both sides of the core two wings or PSs, each being the

result of a pair of interpenetrated boundary layers, are formed. In these wings the plasma velocity is not uniform but sheared. It decreases from the maximum value V_0 assumed in the core to a minimum value in central region of the wings. In our model the plasma bulk velocity tends to zero for $y \to \pm y_\infty$. The width of the central core depends on the two input parameters y_1 and y_2 as well as on the temperatures of the stagnant species, T_{e1} and T_{i1}. Moreover, within the wings there is a flow reversal where the plasma is convecting in the direction opposite to the motion of the core. Our results show that, like in hydrodynamical piston flows, the forward motion of a plasma element (a slab in this case) drives the backward motion of the adjacent layers.

The distributions of plasma and fields are not the same on the left-hand side and on the right-hand side. One side the PS is thinner and has an embedded CS within which sharp variation of the plasma parameters have been obtained. On the opposite side a thicker PS is formed with a smoother transition profile. It also embeds a small-scale current sheet with sharp variations of the potential and density. In case (A) of a core moving with a positive velocity ($V_0 > 0$), the sharper transition is formed on the right-hand side ($y = y_2$). When the sign of the core's velocity is changed ($V_0 < 0$) but the direction of the external magnetic field is kept the same, the two PSs and their interpenetrated CSs interchange position. Our kinetic model demonstrates that the distributions of the plasma density, bulk velocity, and electromagnetic fields inside a moving slab depend on the sign of the velocity with respect to the external magnetic field. Similar results were already found by Sestero,[14] Roth,[15,16] Kuznetsova *et al.*,[28] and De Keyser and Roth[29–32] in their 1D kinetic models of tangential discontinuities. These authors show that the width of the transition layer formed at the interface between moving and stagnant plasmas depends on the sign of the asymptotic velocity, an effect due to the electric field.

The electric field is enhanced inside the thin current sheets embedded into the wings of the moving plasma slab. Strong electric currents are also present. Nevertheless, the bulk velocity of the plasma as a whole is slightly changed inside the CSs as the resulting electric current flow is mainly of electronic nature (see the lower panels of Figs. 7 and 13). This demonstrates that strong perpendicular electric fields do not necessarily drive a strong cross-B plasma flow (or *jetting*), while strong transversal plasma flow always correspond to an enhanced perpendicular (convection) electric field.[20,34] Similar conclusions were reached recently in the framework of the MHD approximation of plasma physics.[35]

Spatial gradients of high-speed flows directed Earthward in the midtail plasma sheet have recently been determined by Nakamura *et al.*[36] using multipoint observations from the Cluster spacecraft. It was observed that the velocity gradient at the duskward edge of a flow tends to be sharper than that at the dawnward edge. This observation confirms the computation illustrated in Fig. 10 [case (B)] where the geometry of the flow and the magnetic field is the same as that observed by the Cluster spacecraft. Note, however, that Nakamura *et al.*[36] have interpreted their observations as the possible result of an asymmetry in the magnetosphere-ionosphere coupling process associated with the flow.

The kinetic solution found for the convection of a plasma slab across the magnetic field shows that the forward plasma motion drives a backward drift of the background plasma. The boundary layers formed at the interface between moving and stagnant plasma embed microscale structures and are not symmetrical. They interchange position when the direction of slab's motion is reversed. The model gives quantitative assessments of the plasma parameters and fields that are suitable for cross checking with laboratory and *in situ* space plasma investigations.

ACKNOWLEDGMENT

This work was supported by the Belgian Federal Office for Scientific, Technical and Cultural Affairs through ESA PRODEX/Cluster.

APPENDIX A: ANALYTICAL MOMENTS

In order to compute the zero-order moment of the VDF given by Eq. (4) we integrate separately the two terms over the domains of the (H, p_x, μ) space accessible to particles that are passing at $y = \pm y_\infty$. The analytical expressions of the density are given by

$$\rho_{\alpha 1}(\Phi, A_x) = \frac{q_\alpha N_{\alpha 1}}{2} e^{-(q_\alpha \Phi / K T_{\alpha 1})} \{\mathrm{erfc}[\nu_\alpha(A_x, T_{\alpha 1}, A_{x1})] + \mathrm{erfc}[-\nu_\alpha(A_x, T_{\alpha 1}, A_{x2})]\}, \tag{A1}$$

$$\rho_{\alpha 2}(\Phi, A_x) = \frac{q_\alpha N_{\alpha 2}}{2} e^{-(q_\alpha \Phi / K T_{\alpha 2})}\, e^{(q_\alpha A_x V_0 / K T_{\alpha 2})} \times \{\mathrm{erfc}[\gamma_\alpha(A_x, A_{x2})] - \mathrm{erfc}[\gamma_\alpha(A_x, A_{x1})]\}. \tag{A2}$$

The functions $\nu_\alpha(A_x, T, c)$ and $\gamma_\alpha(A_x, c)$ are defined by

$$\nu_\alpha(A_x, T, c) = |q_\alpha| \frac{A_x - c}{\sqrt{2 m_\alpha K T}}, \tag{A3}$$

$$\gamma_\alpha(A_x, c) = -\left[\nu_\alpha(A_x, T_{\alpha 2}, c) + \mathrm{sgn}(q_\alpha) \frac{m_\alpha V_0}{\sqrt{2 m_\alpha K T_{\alpha 2}}}\right]. \tag{A4}$$

$N_{\alpha 1}$, $T_{\alpha 1}$, $N_{\alpha 2}$, $T_{\alpha 2}$ correspond to the asymptotic density and temperature of the stagnant (index "1") and moving plasma slabs (index "2") respectively, erfc is the complementary error function.[37]

The first-order moment of the VDF is equal to the flux of particles which is proportional to the electric current density carried by these charged particles. Only the x component is different from zero. After integration of the VDF specified in Eq. (4), one finds that

$$j_{x\alpha 1}(\Phi, A_x) = J_{\alpha 1} e^{-(q_\alpha \Phi / K T_{\alpha 1})} \times [e^{-[\nu_\alpha(A_x, T_{\alpha 1}, A_{x1})]^2} - e^{-[\nu_\alpha(A_x, T_{\alpha 1}, A_{x2})]^2}], \tag{A5}$$

$$j_{x\alpha 2}(\Phi,A_x) = J_{\alpha 2} e^{-(q_\alpha \Phi/KT_{\alpha 2})}\, e^{(q_\alpha A_x V_0/KT_{\alpha 2})} \times\{V^*_{\alpha 0}\mathrm{erfc}[\gamma(A_x,A_{x2})] + \mathrm{sgn}(q_\alpha) e^{-[\gamma(A_x,A_{x2})]^2} - V^*_{\alpha 0}\mathrm{erfc}[\gamma(A_x,A_{x1})] - \mathrm{sgn}(q_\alpha) e^{-[\gamma(A_x,A_{x1})]^2}\}, \quad \text{(A6)}$$

with

$$J_{\alpha 1} = -|q_\alpha| N_{\alpha 1}\sqrt{\frac{KT_{\alpha 1}}{2\pi m_\alpha}},$$

$$V^*_{\alpha 0} = \sqrt{\frac{\pi m_\alpha}{2KT_{\alpha 2}}} V_0,$$

$$J_{\alpha 2} = q_\alpha N_{\alpha 2}\sqrt{\frac{KT_{\alpha 2}}{2\pi m_\alpha}}.$$

APPENDIX B: SCALING FACTORS

The equations solved numerically in Sec. III were normalized. The general rule of normalization is given by

$$P = \lambda_P P^*,$$

where P is the physical quantity, λ_P is the dimensional scaling factor, and P^* is the corresponding nondimensional quantity.

The electric potential is scaled with the potential necessary to accelerate an electron to the reference thermal energy KT_{ref}:

$$\Phi = \lambda_\Phi \Phi^*, \quad \lambda_\Phi = \frac{KT_{\mathrm{ref}}}{e}.$$

The magnetic vector potential is scaled with

$$A_x = \lambda_{A_x} A^*_x, \quad \lambda_{A_x} = \frac{\sqrt{2m_e KT_{\mathrm{ref}}}}{e}$$

and the magnetic induction with a reference magnetic field λ_B:

$$B = \lambda_B B^*.$$

The electric current is scaled with the current carried by electrons moving with the thermal velocity and having the density N_0:

$$\boldsymbol{j} = \lambda_j \boldsymbol{j}^*, \quad \lambda_j = (eN_0)\sqrt{\frac{2KT_{\mathrm{ref}}}{m_e}}.$$

The velocity is scaled with the proton thermal velocity

$$V = \lambda_V V^*, \quad \lambda_V = \sqrt{\frac{2KT_{\mathrm{ref}}}{m_p}}.$$

We have also defined the nondimensional quantities

$$\gamma = \frac{m_e}{m_i}, \quad \tau_e = \frac{T_{\mathrm{ref}}}{T_{e1}}, \quad \tau_{e2} = \frac{T_{\mathrm{ref}}}{T_{e2}},$$

$$\tau_i = \frac{T_{\mathrm{ref}}}{T_{p1}}, \quad \tau_{i2} = \frac{T_{\mathrm{ref}}}{T_{p2}}.$$

T_{ref} is a reference energy equal to 1.5 eV in the computations discussed in Sec. III.

The spatial coordinate perpendicular and parallel to the magnetic field are both scaled with the proton Larmor radius:

$$y = \lambda_y y^*, \quad \lambda_y = r_{\mathrm{Lp}} = \frac{\sqrt{2m_p KT_{\mathrm{ref}}}}{eB},$$

$$z = \lambda_z z^*, \quad \lambda_z = r_{\mathrm{Lp}} = \frac{\sqrt{2m_p KT_{\mathrm{ref}}}}{eB}.$$

[1] T. Hurtig, N. Brenning, and M. A. Raadu, Phys. Plasmas **10**, 4291 (2003).
[2] N. Brenning and C.-G. Fälthammar, Phys. Scr. **70**, 2 (2004); **70**, 153 (2004).
[3] S. I. Krasheninnikov, Phys. Lett. A **283**, 368 (2001).
[4] D. A. D'Ippolito, J. R. Myra, and S. I. Krasheninnikov, Phys. Plasmas **9**, 1 (2002); **9**, 222 (2002).
[5] B. Hultquist and M. Oieroset, *Transport Across the Boundaries of the Magnetosphere* (Kluwer Academic, Dordrecht, 1997).
[6] M. Galvez, Phys. Fluids **30**, 2729 (1987).
[7] W. A. Livesey and P. L. Pritchett, Phys. Fluids B **1**, 914 (1989).
[8] M. Galvez and C. Barnes, Phys. Fluids **31**, 863 (1988).
[9] T. Neubert, R. H. Miller, O. Buneman, and K.-I. Nishikawa, J. Geophys. Res. **97**, 12057 (1992).
[10] K.-I. Nishikawa, J. Geophys. Res. **102**, 17631 (1997).
[11] T. Kitanishi, J.-I. Sakai, K.-I. Nishikawa, and J. Zhao, Phys. Rev. E **53**, 6 (1996); **53**, 6376 (1996).
[12] A. Sestero, Phys. Fluids **7**, 44 (1964).
[13] J. Lemaire and L. F. Burlaga, Astrophys. Space Sci. **45**, 303 (1976).
[14] A. Sestero, Phys. Fluids **9**, 2006 (1966).
[15] M. Roth, J. Atmos. Terr. Phys. **38**, 1065 (1976).
[16] M. Roth, Mémoires de la Classe des Sciences, Acad. Royale de Belgique, Collection 8e, 2ème Série, T XLIV, Fasc. 7, 1984.
[17] M. Roth, J. De Keyzer, and M. Kuznetsova, Space Sci. Rev. **76**, 251 (1996).
[18] L. C. Lee and J. R. Kan, J. Geophys. Res. **84**, 6417 (1979).
[19] M. M. Echim, Ph.D. thesis, Université Catholique de Louvain, Louvain-la-Neuve, 2004.
[20] J. Lemaire, J. Plasma Phys. **33**, 425 (1985).
[21] J. L. Delcroix and A. Bers, *Physique des Plasmas* (Savoirs Actuels Inter Éditions/CNRS Éditions, Paris, 1994), p. 115.
[22] H. Alfvén, *Cosmical Electrodynamics* (Clarendon, Oxford, 1953).
[23] J. Lemaire and M. Scherer, Phys. Fluids **14**, 1683 (1971).
[24] A. A. Vlasov, *Many-Particle Theory and its Application to Plasma* (Gordon and Breach, New York, 1961).
[25] E. C. Whipple, J. Geophys. Res. **82**, 1525 (1977).
[26] M. W. Liemohn and G. V. Khazanov, Phys. Plasmas **5**, 580 (1998).
[27] W. Peter and N. Rostoker, Phys. Fluids **25**, 730 (1982).
[28] M. Kuznetsova, M. Roth, Z. Wang, and M. Ashour-Abdalla, J. Geophys. Res. **99**, 4095 (1994).
[29] J. De Keyser and M. Roth, J. Geophys. Res. **102**, 9543 (1997).
[30] J. De Keyser and M. Roth, J. Geophys. Res. **102**, 19943 (1997).
[31] J. De Keyser and M. Roth, J. Geophys. Res. **103**, 6653 (1998).
[32] J. De Keyser and M. Roth, J. Geophys. Res. **103**, 6663 (1998).
[33] L. J. Cargill, and T. E. Eastman, J. Geophys. Res. **96**, 13763 (1991).
[34] G. Schmidt, Phys. Fluids **3**, 961 (1960).
[35] V. M. Vasyliunas, Geophys. Res. Lett. **28**, 2177 (2001).
[36] R. Nakamura, W. Baumjohann, C. Mouilis, L. M. Kistler, A. Runov, M. Volwerk, Y. Asano, Z. Vörös, T. L. Zhang, B. Klecker, H. Rème, and A. Balogh, Geophys. Res. Lett. **31**, L09804 (2004).
[37] M. Abramowitz and I. A. Stegun, *Handbook of Mathematical Functions* (Dover, New York, 1964).